Layer-Selective Switching of a Double-Layer Perpendicular Magnetic Nanodot Using Microwave Assistance

H. Suto,* T. Nagasawa, K. Kudo, T. Kanao, K. Mizushima, and R. Sato

Corporate Research and Development Center, Toshiba Corporation, Komukai-Toshiba-cho 1, Saiwai-ku, Kawasaki 212-8582, Japan

(Received 9 August 2015; revised manuscript received 5 November 2015; published 12 January 2016)

Layer-selective manipulation of the magnetization direction in a multilayer magnetic structure offers a way to develop a large-capacity magnetic recording device with multiple recording layers. Here, we use a double-layer perpendicular magnetic nanodot consisting of two layers with low and high perpendicular magnetic anisotropy (PMA) and show that layer-selective magnetization switching can be accomplished by utilizing a microwave-assisted magnetization switching technique. Since the low- and high-PMA magnetic layers have different ferromagnetic resonance frequencies, their magnetization excitation that reduces the switching field can be individually induced by adjusting the frequency of the applied microwave field (f_{rf}), and this principle allows f_{rf} to select the layer to be switched. In addition, by measuring thermally excited ferromagnetic-resonance signals from the nanodot, we find that the magnetization dynamics of the two PMA layers couple through interactions, and we identify the excitation modes responsible for the layer-selective magnetization switching.

DOI: 10.1103/PhysRevApplied.5.014003

I. INTRODUCTION

Magnetization switching has long been studied because it is a fundamental physical phenomenon as well as a core technology for magnetic recording that plays a key role in information-storage technology. Conventionally, magnetization switching has been conducted by applying a magnetic field, which hard disk drives (HDDs) employ for switching magnetic data bits on media, i.e., for writing data. To keep up with the rapid increase in data volumes, there is a strong demand to increase the recording density. Planar miniaturization of data bits, however, will eventually meet the superparamagnetic limit where the thermal stability of data bits becomes insufficient [1,2].

Given these circumstances, three-dimensional magnetic recording with multiple recording layers has been proposed [3–13]. According to previous studies on field-induced switching for three-dimensional devices [3–6], when each of the multiple recording layers is provided with a different coercive field (H_c), magnetization manipulation is accomplished by switching the layers sequentially in order from the one with the largest H_c to the one with the lowest H_c. Such multistep writing, however, significantly slows device operation.

To solve this problem, a writing method that can conduct single-step magnetization switching selectively in a specific recording layer is required. To realize this, we focus on microwave-assisted magnetization switching (MAS) [7–9,13–23]. Recent studies on MAS have revealed that reduction in the switching field (H_{sw}) of a magnet depends on the frequency of the applied microwave field (f_{rf}), which is related to the ferromagnetic-resonance (FMR) frequency of the magnet [18–23]. Therefore, when each recording layer is provided with a different FMR frequency, the magnetization of a specific layer is expected to reverse by adjusting f_{rf}.

It should also be mentioned that MAS is currently being explored as a writing method for next-generation HDDs with a single recording layer because H_{sw} reduction realized by MAS is beneficial for writing on high-coercivity media [2]. By using a spin-torque oscillator that generates a microwave magnetic field, and by placing it inside a write-head element, magnetic recording based on MAS becomes compatible with the conventional HDD technology. In addition, multilayer magnetoresistive random-access memory that uses spin-torque oscillators for layer-selective writing has also been proposed [24,25].

In this research, we use a double-layer perpendicular magnetic nanodot and demonstrate that MAS can realize layer-selective magnetization switching. Furthermore, by measuring thermally excited FMR spectra, we identify the magnetization dynamics responsible for the layer-selective magnetization switching.

II. EXPERIMENTAL DETAILS

A. Film preparation

We use a magnetron sputtering system to fabricate a tunnel-magnetoresistive (TMR) film shown in Fig. 1(a), which consists of two CoFe-based in-plane magnetic layers (IL_1 and IL_2), a MgO barrier layer, and two Co/Pt-multilayer-based perpendicular magnetic layers (LL and UL). LL is designed to have a higher perpendicular magnetic

*hirofumi.suto@toshiba.co.jp

 © 2016 American Physical Society

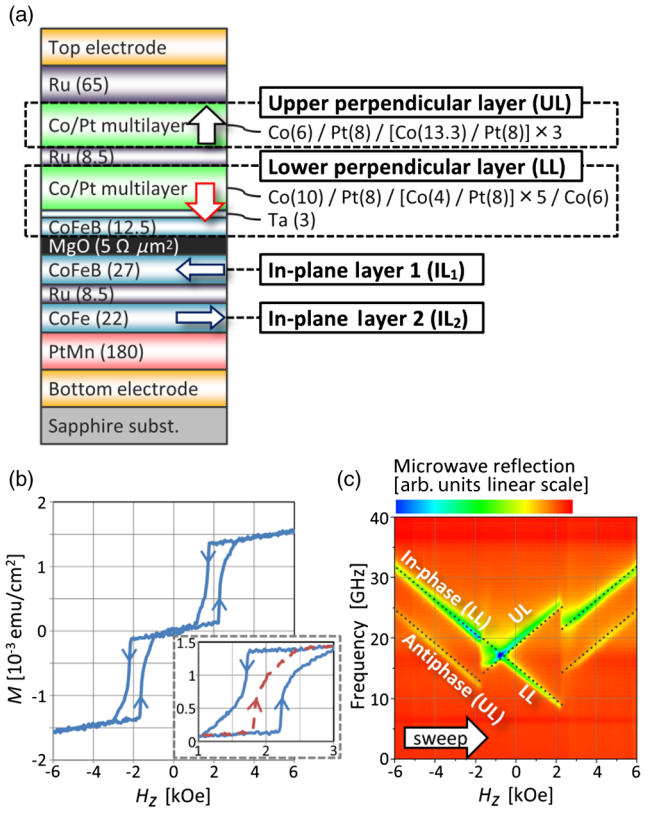

FIG. 1. (a) Stacking structure of the TMR film consisting of two perpendicular magnetic layers, a MgO tunnel barrier, and two in-plane magnetic layers. The order of layers shown for the Pt/Co multilayers is from bottom to top. All thicknesses are given in angstroms except for the MgO layer where the area product value is given. (b) Perpendicular *M*-*H* loop for the film sample. In the inset, the dashed line shows a minor loop of UL switching. (c) H_z dependence of VNA reflection spectra for the film sample. Dashed lines show the fitting results using Eqs. (1) and (2).

anisotropy than UL by tuning the thicknesses of the Co/Pt multilayer. In later experiments, we pattern this TMR film into a nanodot and study the switching behavior of LL and UL, in which IL_1 and IL_2 serve as sensing layers to detect the switching through the magnetoresistive (MR) effect. IL_1 and IL_2 are antiferromagnetically coupled by a Ruderman-Kittel-Kasuya-Yosida-like exchange interaction through a Ru layer, so that they have an antiferromagnetic configuration and cancel the stray fields that arise in the nanodot sample. IL_2 is pinned by a PtMn layer. LL and UL are also antiferromagnetically coupled through a Ru layer. This antiferromagnetic coupling is intended to compensate for the perpendicular stray fields between LL and UL that arise in the nanodot sample and favor a ferromagnetic configuration. After deposition, the film is annealed at 300 °C for 1 h in an in-plane magnetic field of 6400 Oe along the $+x$ direction.

B. Film characterization

The magnetic configuration of the film is confirmed using a vibrating sample magnetometer (VSM) [Fig. 1(b)]. Abrupt changes at a magnetic field along the z direction (H_z) of ± 1700 Oe and ± 2200 Oe correspond to UL and LL switching, respectively. Because LL and UL are antiferromagnetically coupled and have almost the same areal magnetic moment, the net magnetization becomes zero at remanence. The slope over the measured H_z range originates from the gradual tilting of magnetization in IL_1 and IL_2.

The magnetic characteristics of UL and LL are also evaluated by vector-network-analyzer-FMR (VNA-FMR) measurement [Fig. 1(c)]. Discontinuities of the spectra at $H_z = -1700$ and $+2200$ Oe reflect UL and LL switching, respectively, which agrees with the switching fields obtained by the VSM measurement. The FMR frequencies of such a coupled system are described by the equations shown below. When the two layers are in a ferromagnetic configuration with both magnetization directions being the $+z$ direction,

$$f_{\mathrm{FMR}} = (\gamma/2\pi)\Big|(H_{\mathrm{ferro}}^{\mathrm{LL}} + H_{\mathrm{ferro}}^{\mathrm{UL}})/2 \pm \sqrt{(H_{\mathrm{ferro}}^{\mathrm{LL}} - H_{\mathrm{ferro}}^{\mathrm{UL}})^2/4 + H_{\mathrm{Ru}}^{\mathrm{LL}} H_{\mathrm{Ru}}^{\mathrm{UL}}}\Big|, \quad (1)$$

where $H_{\mathrm{ferro}}^{n} = H_z + H_k^n + H_{\mathrm{Ru}}^n$ ($n = \mathrm{LL},\ \mathrm{UL}$) is the perpendicular effective field acting on the layer n, H_k^n is the effective perpendicular magnetic anisotropy, and H_{Ru}^n is the coupling field. The symbol γ is the gyromagnetic ratio. The lower of these two frequencies is an antiphase mode in which the two magnetizations precess in opposite directions, and the higher is an in-phase mode in which the two magnetizations precess in alignment. For an asymmetric system, such as our TMR film in which LL and UL have different H_k and H_{Ru}, the layer with a higher intrinsic FMR frequency (LL in our sample) is expected to have a larger precession amplitude for the in-phase mode, and the other layer with a lower intrinsic FMR frequency (UL) is expected to have a larger precession amplitude for the antiphase mode. When the two layers are in an antiferromagnetic configuration with the LL and UL magnetization directions being in the $-z$ and $+z$ directions, respectively,

$$f_{\mathrm{FMR}} = (\gamma/2\pi)\Big||H_{\mathrm{AF}}^{\mathrm{LL}} - H_{\mathrm{AF}}^{\mathrm{UL}}|/2 \pm \sqrt{(H_{\mathrm{AF}}^{\mathrm{LL}} + H_{\mathrm{AF}}^{\mathrm{UL}})^2/4 - H_{\mathrm{Ru}}^{\mathrm{LL}} H_{\mathrm{Ru}}^{\mathrm{UL}}}\Big|, \quad (2)$$

where $H_{\mathrm{AF}}^{\mathrm{LL}} = -H_z + H_k^{\mathrm{LL}} - H_{\mathrm{Ru}}^{\mathrm{LL}}$ and $H_{\mathrm{AF}}^{\mathrm{UL}} = H_z + H_k^{\mathrm{UL}} - H_{\mathrm{Ru}}^{\mathrm{UL}}$. For an antiferromagnetic configuration, the interaction has little influence on the magnetization dynamics because the two magnetizations have the opposite precession direction. Dashed lines in Fig. 1(c) show the fitting results using these two equations, which yield the parameters H_k^n and H_{Ru}^n shown in Table I. The value of $H_{\mathrm{Ru}}^{\mathrm{UL}}$ is almost consistent with the VSM measurement [Fig. 1(b), inset] in which the center of the minor loop of UL switching is shifted to $H_z = +1800$ Oe because of the coupling.

TABLE I. Magnetic properties of a film sample evaluated by VNA-FMR measurement.

Layer	H_k	H_{Ru} (Minus values mean antiferromagnetic coupling)
UL	4800 Oe	−1900 Oe
LL	5400 Oe	−100 Oe

C. Nanodot sample fabrication and measurement setup

Figure 2(a) shows a sample structure and experimental setup used for the MAS experiment. The TMR film is patterned into a magnetic tunnel junction (MTJ) nanodot with a diameter of 200 nm by electron-beam lithography and Ar ion milling. The milling process removes the film to the middle of the PtMn layer outside the nanodot. The sample has two terminals. The first one is used for applying a microwave magnetic field to the MTJ. It connects with a G-S_1 (ground-signal) coplanar waveguide that consists of the bottom electrode and is shorted near the MTJ. Applying an electric microwave signal to this waveguide generates a linearly polarized microwave magnetic field along the x direction. A pulsed microwave signal with a pulse width of 2 μs and a repetition frequency of 100 Hz is used to avoid a temperature rise of the sample. The amplitude of the microwave field is set to 253 Oe. The other terminal is used for detecting magnetization switching. It connects to a G-S_2-G coplanar waveguide that consists of the top and bottom electrode and is terminated by the MTJ. By applying a direct current (I_{dc}) to this terminal, the sample resistance that represents the angle between LL and IL_1 magnetizations through the magnetoresistive effect is measured.

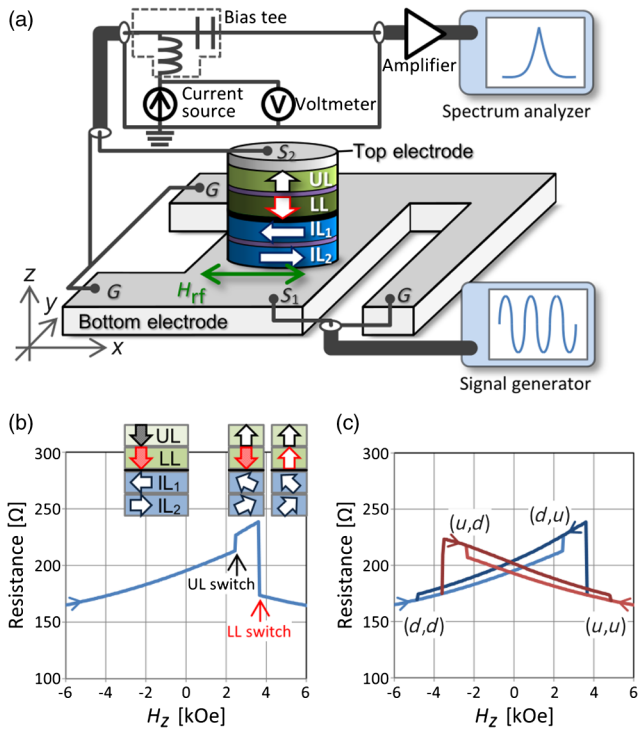

FIG. 2 (a) Sample structure and experimental setup. (b) H_z dependence of sample resistance obtained by applying $I_{dc} = +5$ μA. Schematics represent the magnetization configuration of the sample. (c) Resistance loops for all four magnetization states (d, d), (u, d), (d, u), and (u, u).

Figure 2(b) shows the H_z dependence of the sample resistance without a microwave field. The H_z is increased at intervals of 10 Oe per 0.2 s, and the sample resistance is measured after each increase. For $H_z = -6000$ to $+2500$ Oe, the resistance gradually increases because the H_z tilts the IL_1 magnetization while LL and UL are in the $-z$ direction. At $H_z = +2500$ Oe, the resistance increases abruptly because UL switching occurs and reverses its stray field acting on IL_1, which changes the IL_1 magnetization direction. At $H_z = +3500$ Oe, the resistance decreases abruptly because of the switching of LL, which is placed directly above the MgO barrier. By changing the sweep direction and the initial state, we measure the resistance loops of the four magnetization states: a combination of up and down states in LL and UL, as shown in Fig. 2(c). This result shows that the magnetization configuration of LL and UL is distinguished by measuring the resistance. When the in-plane layers (ILs) are tilted by H_z, they generate z-direction stray fields acting on LL and UL. By modeling the sample structure using $1 \times 1 \times 1$-nm cells and assuming the saturation magnetization of CoFeB to be 1200 emu cm^{-3}, the z-direction stray field from IL_1 to UL is estimated to be at most 180 Oe within the H_z range of this study (−6000 to 6000 Oe). Because IL_2 also generates the z-direction stray field, the measured H_{sw} may deviate by a few hundred Oe from the actual z-direction field acting on LL and UL.

Furthermore, this setup can measure a high-frequency component of the sample resistance (referred to as an MTJ signal) using a spectrum analyzer. The MTJ signal reflects the thermally excited magnetization dynamics of LL and IL_1. When acquiring the MTJ signals, no microwave field is applied. All measurements are carried out at room temperature. For convenience, we introduce the symbol expression (u or d, u or d), in which "u" and "d" denote the up and down states of LL and UL in that order.

III. EXPERIMENTAL RESULTS

Here, we study MAS from two antiferromagnetic configurations, namely, the transition from (d, u) and (u, d) to (u, u), in which a layer with a down state reverses. Then, we study MAS from a ferromagnetic configuration (d, d) in which a layer to be switched is selected by adjusting f_{rf}.

A. Switching of LL from an antiferromagnetic configuration

Figure 3(a) shows the H_z dependence of the sample resistance obtained by applying microwave fields for several f_{rf}

values, together with one without a microwave field. The initial state is (d, u). Switching of LL detected by the resistance drop occurs at a different H_z depending on f_{rf}. This result shows that the switching is influenced by microwave fields. Figure 3(b) summarizes the H_{sw} and its distribution with respect to f_{rf}. The values without microwave fields are plotted at $f_{rf} = 0$ GHz. The result is similar to the typical MAS behavior of a perpendicular magnetic nanodot in which H_{sw} decreases as f_{rf} increases and abruptly increases at a critical frequency. The result shows two abrupt H_{sw} increases at 10.5 and 13 GHz. Such MAS behavior with multiple critical frequencies is observed when multiple excitation modes contribute to H_{sw} reduction, and critical frequencies correspond to mode transitions [21].

Figure 3(c) shows the corresponding H_z dependence of the power spectrum density (PSD) of the MTJ signals that reflect the thermally excited magnetization dynamics of LL and IL_1. The discontinuity of the PSD at $H_z = 3200$ Oe reflects LL switching. This value is smaller than the H_{sw} obtained from the resistance measurement because the larger I_{dc} raises the sample temperature in the PSD measurement. Signals having a linearly decreasing frequency with respect to H_z are attributed to the magnetization dynamics of LL (LL-1, LL-2, and LL-3). If the LL and UL magnetizations move cooperatively coupled by the

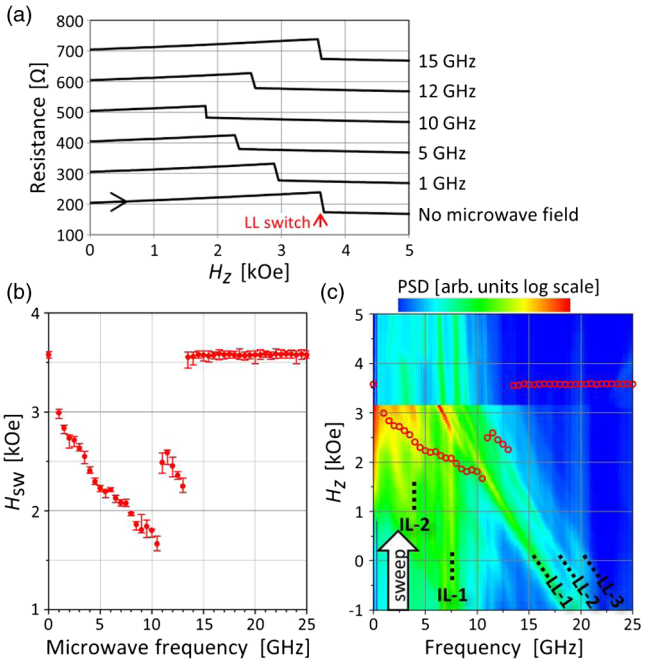

FIG. 3. (a) H_z dependence of sample resistance with initial state being (d, u) for several values of f_{rf}. Current I_{dc} is set to $+5$ μA. Each curve is offset for clarity. (b) f_{rf} dependence of H_{sw}. Circles and error bars represent the average, maximum, and minimum values among 20 repeated measurements. (c) MTJ signal spectra obtained by applying $I_{dc} = +1.6$ mA. During spectra measurement, H_z is swept in the upward direction. The discontinuity in spectra at $H_z = +3200$ Oe corresponds to LL switching. Open circles represent the average H_{sw} shown in (b).

exchange and dipolar interactions, signals characteristic to UL that are expected to have the opposite slope with respect to H_z should appear. Such signals, however, are not observed, indicating that the LL and UL magnetizations move almost independently. The lowest LL mode (LL-1) is a uniform mode and the others are higher-order spin-wave modes [20,26]. The LL-1 mode frequency of 16 GHz at $H_z = 0$ Oe is higher than the LL-FMR frequency of 15 GHz for the film [Fig. 1(c)]. This discrepancy results from patterning owing to the following two factors. The perpendicular demagnetizing fields decrease, which increases the FMR frequency, and the perpendicular stray fields between UL and LL arise, which decreases the FMR frequency for the antiferromagnetic configuration. Since the former has a larger influence, the FMR frequency of the nanodot sample increases. A signal around 7.5 GHz (IL-1) that has an almost constant frequency with respect to H_z is attributed to the magnetization dynamics of IL_1 [21,26]. Strictly speaking, the IL_1 magnetization moves cooperatively with IL_2 as a result of the coupling because the magnetization dynamics of in-plane magnetic layers couple even in an antiferromagnetic configuration, owing to their elliptical precession trajectory [26,27]. The FMR frequency of the coupled dynamics of the in-plane magnetic layers (ILs) is dominantly determined by the in-plane effective field and thus is independent of H_z as long as H_z is so weak that the ILs magnetizations are almost in the in-plane direction. Other signals appear that have an almost constant frequency, such as IL-2. They may be spatially inhomogeneous modes such as an edge-localized mode, which is expected to show a lower frequency than the main uniform mode [28]. Here, we do not elucidate their details because it is beyond the scope of this paper. Below 10 GHz, the H_{sw} reduction cannot be assigned to a certain FMR mode. The FMR modes of ILs may contribute to the LL switching through dipolar interaction because several ILs FMR modes exist in this f_{rf} range. Above 10 GHz up to the first critical frequency, the H_{sw}-f_{rf} curve coincides with the LL-1 mode, and above the first critical frequency up to the second critical frequency, it coincides with the LL-2 mode, indicating that the H_{sw} reduction originates from the excitation of these modes. Theoretically, H_{sw} under microwave assistance is expected to differ from the condition of thermally excited FMR owing to the nonlinearity of magnetization excitation. However, as seen in Fig. 3(c), these two almost coincide, and such coincidence was also found in our previous experimental study on MAS of a single-layer perpendicular magnetic nanodot [21]. We are presently investigating the reason for this discrepancy between the theory and experiment.

B. Switching of UL from an antiferromagnetic configuration

We evaluate the MAS of UL from (u, d). Figure 4(a) compares typical H_z dependences of the sample resistance.

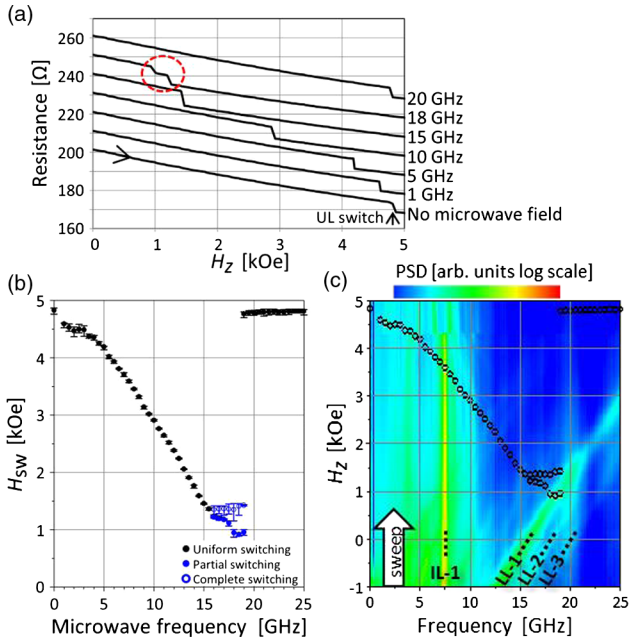

FIG. 4. (a) H_z dependence of sample resistance with initial state being (u, d) for several values of f_{rf}. Current I_{dc} is set to $+5$ μA. Each curve is offset for clarity. The dashed circle indicates an intermediate resistance, which corresponds to partial switching of UL. (b) f_{rf} dependence of H_{sw}. Circles and error bars represent the average, maximum, and minimum values among 20 repeated measurements. For $f_{rf} = 16$ to 19 GHz, filled circles and open circles represent partial switching and subsequent complete switching, respectively. (c) MTJ signal spectra obtained by applying $I_{dc} = +1.6$ mA. The discontinuity in spectra at $H_z = +4300$ Oe corresponds to UL switching. Open circles represent the average H_{sw} shown in (b).

The H_{sw} of UL detected by the resistance drop decreases as f_{rf} increases. At $f_{rf} = 18$ GHz, switching of part of UL occurs, which appears as an intermediate resistance. Figure 4(b) shows the f_{rf} dependence of the H_{sw} and its distribution. For $f_{rf} = 16$ to 19 GHz, two H_{sw}-f_{rf} plots represent partial switching and subsequent complete switching. Figure 4(c) shows the corresponding H_z dependence of the PSD of the MTJ signals, which is a mirror image of Fig. 3(c) with respect to $H_z = 0$ Oe because the (d, u) and (u, d) configurations are symmetric. The discontinuity of the PSD at $H_z = 4300$ Oe reflects UL switching. Several signals corresponding to the FMR modes of ILs and LL appear just as in Fig. 3(c). Since the UL dynamics cannot be revealed through the MTJ signals, no signal coincides with the H_{sw}-f_{rf} curve of UL.

C. Layer-selective switching of UL and LL from a ferromagnetic configuration

We evaluate MAS from the ferromagnetic configuration. The sample is initialized to (d, d) and transition to (u, d), (d, u), or (u, u) occurs depending on f_{rf}. Figure 5(a) compares typical H_z dependences of the sample resistance.

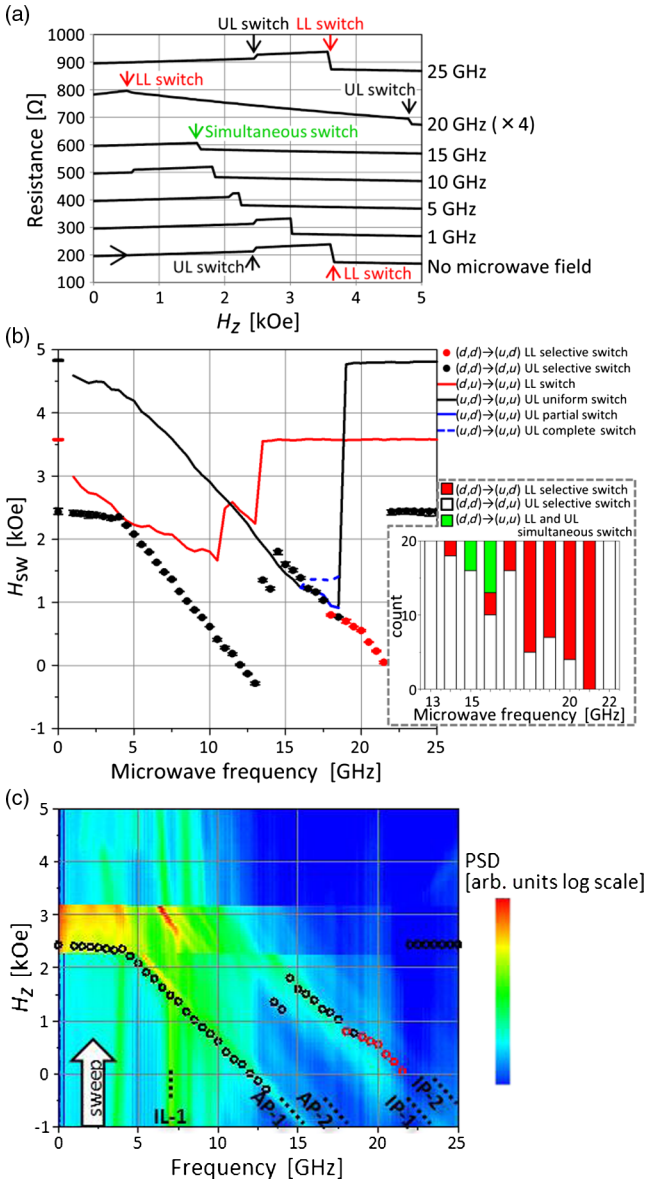

FIG. 5 (a) H_z dependence of sample resistance with the initial state being (d, d) obtained for several values of f_{rf}. The current I_{dc} is set to $+5$ μA. The curve for $f_{rf} = 20$ GHz is multiplied by 4 and each curve is offset for clarity. (b) f_{rf} dependence of H_{sw}. Circles and error bars represent the average, maximum, and minimum values among 20 repeated measurements. Lines represent H_{sw} of LL and UL from the (d, u) and (u, d) configurations [the same results shown in Figs. 3(b) and 4(b)]. The inset shows the number of occurrences of LL, UL, and simultaneous switching. (c) MTJ signal spectra obtained by applying $I_{dc} = +1.6$ mA. The discontinuities in spectra at $H_z = +2300$ and $+3200$ Oe correspond to UL and LL switching. Open circles represent the average H_{sw} shown in (b).

For $f_{rf} = 1$, 5, and 10 GHz, UL reverses first, and for $f_{rf} = 15$ GHz, LL and UL reverse simultaneously. For $f_{rf} = 20$ GHz, LL reverses first, which shows that layer-selective switching can be accomplished by selecting f_{rf}. The resistance change by the LL switching is small because

it occurs around $H_z = 500$ Oe where the resistance curves of the (d, d) and (u, d) configurations are close [Fig. 2(c)]. For $f_{rf} = 25$ GHz, f_{rf} is so high that the microwave field has no influence and UL reverses first. Figure 5(b) summarizes the kind of switching, corresponding H_{sw}, and H_{sw} distribution with respect to f_{rf}. The H_{sw} from the antiferromagnetic configuration [Figs. 3(b) and 4(b)] is also plotted. For $f_{rf} = 1$ to 13 GHz, UL always reverses as in the case without microwave fields, and its H_{sw} gradually decreases as f_{rf} increases. At $f_{rf} = 14$ GHz, H_{sw} increases abruptly and the switching of LL, UL, or both occurs stochastically up to 20 GHz. In this frequency range, the kind of switching that occurs most in 20 repeated measurements at a certain f_{rf} is plotted for simplicity. Note that regardless of the layer to be switched, H_{sw} is almost the same (data not shown). The inset shows the number of occurrences of these three kinds of switching. At $f_{rf} = 15$ and 16 GHz, simultaneous switching occasionally occurs. The experimental procedure, however, cannot determine whether the two layers reverse at once or sequentially one by one in a short period of time, and it is probable that LL reverses first followed by UL switching, because the switching of UL from (u, d) occurs under a similar condition [black line in Fig. 5(b)]. Sequential switching in the opposite order can be ruled out because the switching of LL from (d, u) requires much higher H_z [red line in Fig. 5(b)]. The inset shows an overall tendency that the occurrence of LL switching increases as f_{rf} increases, and at $f_{rf} = 21$ GHz, LL reverses without fail.

Figure 5(c) shows the corresponding H_z dependence of the PSD of the MTJ signals. The discontinuities of the PSD at $H_z = 2300$ and 3200 Oe reflect UL and LL switching, respectively. Different from the previous two antiferromagnetic cases, two major signals having linearly decreasing frequency with respect to H_z (AP-1 and IP-1) appear. This is explained by the fact that LL and UL move cooperatively as a result of the interaction, and they are assigned to uniform antiphase (AP-1) and in-phase (IP-1) coupled FMR modes. Higher-order modes (AP-2 and IP-2) also appear. The frequencies of the uniform modes are 12.5 and 20 GHz at $H_z = 0$ Oe. These values are higher than those for the film estimated at 7 and 15 GHz by extrapolating the FMR frequencies in the ferromagnetic configuration [Fig. 1(c)]. These discrepancies are larger than those for the antiferromagnetic cases because two factors—demagnetizing field and perpendicular stray field—resulting from the patterning both increase the FMR frequencies. For $f_{rf} = 4$ to 13 GHz, the H_{sw}-f_{rf} curve coincides with the AP-1 mode, indicating that the excitation of this mode accounts for this UL switching. This coincidence is reasonable because UL has a lower intrinsic FMR frequency and UL magnetization is expected to be preferentially excited in the AP-1 mode, according to the discussion in Sec. II (B). Above $f_{rf} = 15$ GHz, the H_{sw}-f_{rf} curve follows the IP-1 mode, indicating that the MAS in this f_{rf} range originates from

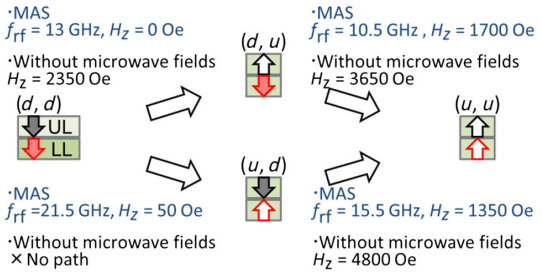

FIG. 6. Manipulation of magnetization states with and without microwave assistance.

excitation of the IP-1 mode. The H_{sw}-f_{rf} curve shifts to the higher frequency side where LL switching becomes dominant around $f_{rf} = 18$ GHz. This suggests that a higher-order mode near the IP-1 mode is excited, although the H_{sw}-f_{rf} curve does not coincide exactly with the MTJ signals.

Because of the stochastic switching, infallible layer-selective switching of LL occurs in a narrow f_{rf} range around 21 GHz. We believe that the interactions between UL and LL might be responsible for this. Although the magnetization is expected to be preferentially excited in the in-phase mode excitation for $f_{rf} = 15$ to 21 GHz, UL is excited simultaneously because of the interactions, and this UL excitation sometimes becomes sufficient for switching. This leads to the stochastic switching of LL and UL. If the coupling is weak enough, magnetization excitation of LL is much stronger than that of UL, which leads to infallible switching of LL. Thus, tailoring the interactions by selecting the magnetic material, controlling the thickness of magnetic layers, and adjusting the exchange interaction might make it simpler to perform layer-selective MAS—one excitation mode corresponds to the switching of one magnetic layer—and realize a robust manipulation of the magnetization direction.

Figure 6 summarizes magnetization switching of the double-layer magnetic nanodot with and without microwave assistance. The most significant advance reported in this paper is the transition from (d, d) to (u, d) realized by MAS. Without a microwave field, this manipulation requires $(d, d) \rightarrow (d, u) \rightarrow (u, u) \rightarrow (u, d)$ transitions. In addition, the H_{sw} required for each transition is reduced by MAS, and manipulating all four states requires H_z of 1700 Oe at most, whereas it requires H_z of 4800 Oe without microwave assistance.

IV. SUMMARY

In summary, we demonstrate that MAS can realize single-step layer-selective magnetization switching of a double-layer perpendicular magnetic nanodot consisting of a LL with a higher PMA and an UL with a lower PMA. The MTJ signal measurements reveal that magnetization dynamics of the two layers are coupled when they have

a ferromagnetic configuration. Exciting the antiphase coupled FMR mode by microwave fields reduces the H_{sw} of UL, while exciting the in-phase coupled mode reduces the H_{sw} of LL, which allows f_{rf} to select the layer to be switched. MAS also reduces the H_{sw} regarding the UL and LL switching from the antiferromagnetic configuration, and the manipulation of all four magnetization states can be conducted with a smaller H_z.

ACKNOWLEDGMENTS

This work was supported by Strategic Promotion of Innovative Research and Development from Japan Science and Technology Agency, JST.

[1] A. Moser, K. Takano, D. T. Margulies, M. Albrecht, Y. Sonobe, Y. Ikeda, S. Sun, and E. E. Fullerton, Magnetic recording: Advancing into the future, J. Phys. D **35**, R157 (2002).

[2] Y. Shiroishi, K. Fukuda, I. Tagawa, H. Iwasaki, S. Takenoiri, H. Tanaka, H. Mutoh, and N. Yoshikawa, Future options for HDD storage, IEEE Trans. Magn. **45**, 3816 (2009).

[3] M. Albrecht, G. Hu, A. Moser, O. Hellwig, and B. D. Terris, Magnetic dot arrays with multiple storage layers, J. Appl. Phys. **97**, 103910 (2005).

[4] V. Baltz, S. Landis, B. Rodmacq, and B. Dieny, Multilevel magnetic media in continuous and patterned films with out-of-plane magnetization, J. Magn. Magn. Mater. **290–291**, 1286 (2005).

[5] S. Khizroev, Y. Hijazi, N. Amos, R. Chomko, and D. Litvinov, Physics considerations in the design of three-dimensional and multilevel magnetic recording, J. Appl. Phys. **100**, 063907 (2006).

[6] N. Amos, J. Butler, B. Lee, M. H. Shachar, B. Hu, Y. Tian, J. Hong, D. Garcia, R. M. Ikkawi, R. C. Haddon, D. Litvinov, and S. Khizroev, Multilevel-3D bit patterned magnetic media with 8 signal levels per nanocolumn, PLoS One **7**, e40134 (2012).

[7] G. Winkler, D. Suess, J. Lee, J. Fidler, M. A. Bashir, J. Dean, A. Goncharov, G. Hrkac, S. Bance, and T. Schrefl, Microwave-assisted three-dimensional multilayer magnetic recording, Appl. Phys. Lett. **94**, 232501 (2009).

[8] S. Li, B. Livshitz, H. N. Bertram, E. E. Fullerton, and V. Lomakin, Microwave-assisted magnetization reversal and multilevel recording in composite media, J. Appl. Phys. **105**, 07B909 (2009).

[9] T. Tanaka, Y. Otsuka, Y. Furomoto, K. Matsuyama, and Y. Nozaki, Selective magnetization switching with microwave assistance for three-dimensional magnetic recording, J. Appl. Phys. **113**, 143908 (2013).

[10] R. Sato, K. Mizushima, T. Nagasawa, and K. Kudo, Three-dimensional magnetic recording and reproducing apparatus including a plurality of magnetic layers having different resonant frequencies, U.S. Patent No. 9,001,466, 7 April 2015.

[11] T. Yang, H. Suto, T. Nagasawa, K. Kudo, K. Mizushima, and R. Sato, Readout method from antiferromagnetically coupled perpendicular magnetic recording media using ferromagnetic resonance, J. Appl. Phys. **114**, 213901 (2013).

[12] H. Suto, T. Nagasawa, K. Kudo, K. Mizushima, and R. Sato, Nanoscale layer-selective readout of magnetization direction from a magnetic multilayer using a spin-torque oscillator, Nanotechnology **25**, 245501 (2014).

[13] S. Okamoto, N. Kikuchi, M. Furuta, O. Kitakami, and T. Shimatsu, Microwave assisted magnetic recording technologies and related physics, J. Phys. D **48**, 353001 (2015).

[14] C. Thirion, W. Wernsdorfer, and D. Mailly, Switching of magnetization by non-linear resonance studied in single nanoparticles, Nat. Mater. **2**, 524 (2003).

[15] J.-G. Zhu, X. Zhu, and Y. Tang, Microwave assisted magnetic recording, IEEE Trans. Magn. **44**, 125 (2008).

[16] Y. Nozaki, M. Ohta, S. Taharazako, K. Tateishi, S. Yoshimura, and K. Matsuyama, Magnetic force microscopy study of microwave-assisted magnetization reversal in submicron-scale ferromagnetic particles, Appl. Phys. Lett. **91**, 082510 (2007).

[17] H. T. Nembach, P. M. Pimentel, S. J. Hermsdoerfer, B. Leven, B. Hillebrands, and S. O. Demokritov, Microwave assisted switching in a $Ni_{81}Fe_{19}$ ellipsoid, Appl. Phys. Lett. **90**, 062503 (2007).

[18] S. Okamoto, N. Kikuchi, M. Furuta, O. Kitakami, and T. Shimatsu, Significant reduction of switching field and its distribution in Co/Pt nanodots with assistance of radio frequency field, Appl. Phys. Express **5**, 093005 (2012).

[19] S. Okamoto, N. Kikuchi, M. Furuta, O. Kitakami, and T. Shimatsu, Switching Behaviors and Its Dynamics of a Co/Pt Nanodot under the Assistance of rf Fields, Phys. Rev. Lett. **109**, 237209 (2012).

[20] M Furuta, S Okamoto, N Kikuchi, O Kitakami, and T Shimatsu, Size dependence of magnetization switching and its dispersion of Co/Pt nanodots under the assistance of radio frequency fields, J. Appl. Phys. **115**, 133914 (2014).

[21] H. Suto, T. Nagasawa, K. Kudo, K. Mizushima, and R. Sato, Microwave-assisted switching of a single perpendicular magnetic tunnel junction nanodot, Appl. Phys. Express **8**, 023001 (2015).

[22] T. Taniguchi, Magnetization reversal condition for a nanomagnet within a rotating magnetic field, Phys. Rev. B **90**, 024424 (2014).

[23] H. Suto, K. Kudo, T. Nagasawa, T. Kanao, K. Mizushima, R. Sato, S. Okamoto, N. Kikuchi, and O. Kitakami, Theoretical study of thermally activated magnetization switching under microwave assistance: Switching paths and barrier height, Phys. Rev. B **91**, 094401 (2015).

[24] R. Sbiaa, Frequency selection for magnetization switching in spin torque magnetic memory, J. Phys. D **48**, 195001 (2015).

[25] K. Kudo, H. Suto, T. Nagasawa, K. Mizushima, and R. Sato, Resonant magnetization switching induced by spin-torque-driven oscillations and its use in three-dimensional magnetic storage applications, Appl. Phys. Express **8**, 103001 (2015).

[26] S. Tamaru, H. Kubota, K. Yakushiji, M. Konoto, T. Nozaki, A. Fukushima, H. Imamura, T. Taniguchi, H. Arai, S. Tsunegi, S. Yuasa, and Y. Suzuki, Observations of thermally excited ferromagnetic resonance on spin torque oscillators having a perpendicularly magnetized free layer, J. Appl. Phys. **115**, 17C740 (2014).

[27] K. Kudo, T. Nagasawa, H. Suto, T. Yang, K. Mizushima, and R. Sato, Influence of dynamical dipolar coupling on spin-torque-induced excitations in a magnetic tunnel junction nanopillar, J. Appl. Phys. **111**, 07C906 (2012).

[28] K. Miyake, S-M Noh, T. Kaneko, H. Imamura, and M. Sahashi, Study on high-frequency 3-D magnetization precession modes of circular magnetic nano-dots using coplanar wave guide vector network analyzer ferromagnetic resonance, IEEE Trans. Magn. **48**, 1782 (2012).